Springer

Journal of
Mechanical
Science and
Technology

Journal of Mechanical Science and Technology 22 (2008) 565~574

www.springerlink.com/content/1738-494x

The structural variation of the gas diffusion layer and a performance evaluation of polymer electrolyte fuel cells as a function of clamping pressure

Sang Yeop Lee[1], Kwan-Soo Lee[2] and Sukkee Um[2,*]

[1]*Fuel Cell Research Center, Korea Institute of Science and Technology, P.O. Box 131, Cheongryang, Seoul, 130-650, South Korea*
[2]*School of Mechanical Engineering, Hanyang University, 17 Haengdang-Dong, Seongdong-Gu, Seoul, 133-791, South Korea*

(Manuscript Received July 6, 2007; Revised Decemebr 26, 2007; Accepted December 26, 2007)

Abstract

Interfacial contact resistance between gas diffusion layers (GDLs) and bipolar plates (BPs) has a substantial effect on the performance loss of polymer electrolyte fuel cells (PEFCs). Particularly during the final manufacturing process of a fuel cell stack, an externally applied clamping load determines the extent of electrical contact between those two solid components. In order to have the least electrical contact loss, it is highly necessary to keep all PEFC components close each other without causing structural failure of fuel cell stacks. In the present work, we investigated the effect of the clamping pressure on extrinsic properties such as porosity and permeability, which is closely related to mass transfer of reactants. Also, the variance of interfacial electrical resistance was analyzed as a function of the stack clamping pressure or the compressed GDL thickness, which reflects the external clamping load. Then with these experimentally obtained material properties of GDL, computational efforts were made to account for the effect of the clamping pressure on the fuel cell performance.

Keywords: Polymer electrolyte fuel cells; Gas diffusion layer; Mass transfer; Clamping pressure; Electrical resistance

1. Introduction

It is widely known that fuel cells consist of membrane electrode assemblies (MEAs), bipolar plates (BPs), and gas diffusion layers (GDLs) in between and these subcomponents are tightly assembled and compressed to build a single cell or fuel cell stacks as an ultimate electrical power module depending on the electrical power demands/applications. In a working fuel cell system, protons move from anode to cathode through the ionomer membranes, and fuel and air go through oxidation and reduction processes at respective catalyst layers. The ionomer membranes and the catalyst layers are usually prepared together, making MEAs, and are mainly in charge of the proton transfer and electrochemical reactions in PEFCs. Compared to the MEAs, BPs have multi-functional role: gas supply, electron transfer, and ultimate heat and water removal. In harmony with MEA and BP, GDLs also play significant roles as an intermediate reactant carrier from gas chamber to the catalyst layers via porous gas paths, ion and electron transfer medium, and heat and water transport medium. From thermo-fluid science and electrical point of views, GDLs seem to have very similar functions to BPs. However, there is a unique key role in GDLs, "a clamping stress absorber." In the final manufacturing stage of fuel cells, a significant external load is applied to make those core elements close to each other and minimize electrical resistances between them. Other solid parts of fuel cells (i.e., MEA and BP) have negligible extra space to withstand such high stacking pressure, e.g., 10 bar/cm^2. Without the highly porous GDLs (e.g., normally 80% of porosity), fuel cells would not assemble properly and work as an alternative clean

*Corresponding author. Tel.: +82 2 2220 0432, Fax.: +82 2 2220 0432
E-mail address: sukkeeum@hanyang.ac.kr
DOI 10.1007/s12206-007-1211-6

energy power source.

The performance of polymer electrolyte fuel cells (PEFCs) is strongly affected by intrinsic and extrinsic properties of the above-mentioned core fuel cell elements. The intrinsic fuel cell properties include the electronic/ionic conductivities, catalytic activity, thermal conductivity, and so on. The extrinsic properties can be defined as material properties which are strongly associated with the external physical conditions. Porosity, permeability, and the interfacial contact resistance may fall into this category. Before exerting a stacking pressure, for instance, typical carbon based gas diffusion layers have 80% of porosity and the corresponding permeability. As the clamping process proceeds, the carbon paper undergoes a structural deformation process and the porosity, permeability, and mass diffusivity of gas diffusion layers get reduced. This deformation process reveals that the porosity is one of the critical extrinsic material properties as a function of stacking pressure or thickness. It should also be noted that the resultant transport and electrochemical reaction in fuel cells might greatly deviate from design values without these variations, which are closely chained to mass transfer of reactants and the electrochemical kinetics.

Net fuel cell efficiency depends upon another external physical parameter, contact resistance, which is also significantly related to the stacking process of a fuel cell engine. There exists an electrical contact resistance between gas diffusion layers and bipolar plates while electrons are transferred to/from an external circuit. The electrical resistance at the interface can be minimized by applying an external stacking force. The magnitude of the contact resistance is lowered as the interfacial contact area increases in proportion to the clamping load. However, the deformation of the porous gas diffusion layer will interfere with mass transfer of reactants from the gas-feeding channel to the catalyst layers, resulting in a negative effect on the fuel cell efficiency. Excessive clamping pressure results in performance loss due mainly to the narrow-downed diffusion path for mass transfer from gas channels to the catalyst layers and/or the increased possibility of flooding in the GDL parallel to the land of bipolar plate. On the contrary, a less fastened fuel cell stack might have better diffusive fluxes of reactant to the active reaction sites, suppress the possible water flooding, and cause increased electrical resistance between the cells. Therefore, the clamping pressure should be balanced in an optimal manner to obtain the maximum fuel cell efficiency as well as to enhance mass transfer in and out through the gas diffusion layer.

Remarkable experimental and numerical researches have been performed to figure out the effect of clamping pressure on mass transfer through gas diffusion layer in the through-membrane direction and the performance of polymer electrolyte fuel cells. For a practical application of fuel cells, a number of cells are put together in series and then high external compressing pressure (e. g. ~10 bar/cm^2) is applied on both end plates. Under this high pressure, the porous carbon diffusion layer is pressed down and eventually takes on a serious variation in thickness and porosity. These drastic changes of GDL characteristics could have a remarkable effect on the fuel cell performance as experimentally demonstrated by Lee et al. [1]. Mikkola et al. [2] found how the variation of gas permeability in GDL goes through under different clamping pressures, targeting to elucidate the intrinsic characteristics of carbon paper, which is widely used in a fuel cell module. Electrical contact resistance between the carbon paper and its neighboring gas channel has been measured by various research groups [3, 4], since the interfacial electrical resistance reflects the material characteristics of the carbon paper and the bipolar plates and is one of the major factors determining the fuel cell performance.

Gurau et al. [5] developed a two-dimensional computational fluid dynamics model by adding the in-plane direction to the existing one-dimensional models. In their work, a fuel cell domain was divided into three different sub-sections for the computational purpose. Dutta et al. [6] developed a numerical program to predict the mass transport phenomena by prescribing semi-empirical boundary conditions. In 2000 Um et al. [7] suggested a single domain computational fuel cell dynamics (CFCD) model in which flow dynamics, transport phenomena and electrochemical kinetics are integrated together. Um [8] further developed the unified water transport model across the membrane by the aide of the equilibrium water uptake curve in the membrane phase. Following this model, numerical effort including the electron transfer through the solid phase and the electronic potentials across the electrodes has been made by Meng and Wang [9]. Notable three-dimensional modeling on the ionomer membrane has been developed by Berning et al. [10] who assumed full saturation of the ionomer and conducted various parametric

studies to identify the their effects on the fuel cell performance by varying the gas channel width, porosity, and thickness of the gas diffusion layer. Recently, two-phase flow models [11-13] has been made to investigate the water condensing and the resultant water flooding in the GDL which is a serious challenging issue in modern fuel cell research. Particularly, Ugur and Wang [13] developed multi-phase and multi-component model (M-2 model) and they worked on characteristics water transport phenomena in the hydrophobic and hydrophilic nature of gas diffusion layer by changing the contact angle.

In the present study, the effect of the clamping pressure on electrical conductivity, porosity, thickness, gas permeability of a carbon paper GDL is extensively investigated by experimental methods and discussed in detail to identify the relationship between the changes of extrinsic material properties and the fuel cell performance by both experimental and computational predictions. Utilizing the experimentally obtained data accounting for the deformation of GDL by the stacking pressure, a computational fuel cell dynamic (CFCD) program developed by Um et al. [7] was adopted and further modified to implement the measured GDL properties and determine the effect of the electrical resistance on the fuel cell performance curve.

2. Experimental setup & numerical modeling

2.1 Experimental setup

Gas flow in a porous diffusion layer encounters additional flow resistance, which causes momentum loss by the intrinsic characteristics of the porous media. This momentum loss is closely associated with the micro structure, material characteristics, and porosity of gas diffusion layers; however, it is hard to quantify the momentum loss of a fluid in an experiment. Therefore, we need to define a material property that describes the diminution of a vector field through porous media, the so-called "gas permeability" which can be greatly utilized to derive other material properties later in this study.

An integrated test stand was built to determine porosity, permeability, and electrical resistance in an integrated multi-measurement system as schematically shown in Fig. 1. SGL 10 BB carbon papers and graphite plates with 1 inch of O.D. and 0.2 inches of I.D. were filed up as shown in Fig. 2 and the external compressive force was measured by using a load cell which can weigh the external load by 0.1 kg up to maximum 200 kgs. During the compression process, the thickness variation of carbon papers was monitored with a thickness gauge that has a minimal gauging limit of 10 μm. The interfacial electrical resistance between the graphite bipolar plate and the carbon gas diffusion layer was detected with a minimum of $1x10^{-5}$ Ω by using a milli-ohm meter (Agilent Technologies). Gas permeability can be measured by using the data of pressure and flow rate at both ends of a test cell. For this purpose a mass flow controller (Alicat Scientific, Inc.) and a pressure differential gauge with a resolution of 0.001 bar were equipped to the test stand as shown in Fig. 1. For reliable data quality, a test gas was passed through a moisture-removing filter packed with dendrites to eliminate the effect of humidity on the gas permeability.

A single cell experiment was then performed to find out the effect of clamping pressure on cell performance. A series of data collected from the experiment could be utilized to show the quantitative effect of the external clamping load on the 1-5 polarization curve and validate the computational results as well. Basic information on a unit cell system for this study is available in Table 1 and an illustrative sketch of a single cell experimental system is displayed in Fig. 3. Pressurized air flows through a small hole in the center and eventually diffuses out to the atmosphere. The gas permeability of the carbon paper can be calculated by measuring pressure before infusing the pressurized air into the concentric porous media [2], which is detailed in the appendix.

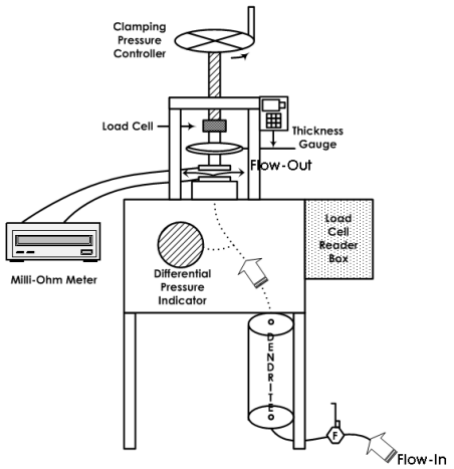

Fig. 1. Schematic configurations of a multi-measurement system.

Table 1. Operating conditions of a single cell test.

Description	Value
Cell Temperature [K]	333
Stoichiometry	1.5/3.0 (Anode/Cathode)
Inlet Relative Humidity [%]	100/100 (Anode/Cathode)
Operating Pressure [atm]	1/1 (Anode/Cathode)
Active area [cm^2]	25

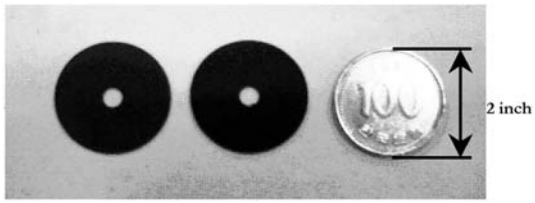

Fig. 2. Samples of carbon paper and graphite.

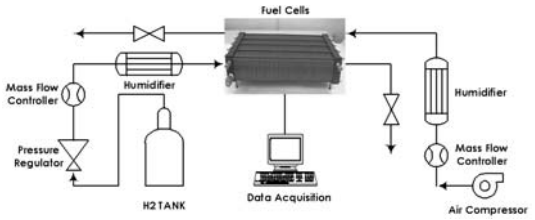

Fig. 3. Sketched illustration of a single cell experimental apparatus.

2.2 Numerical modeling

Fig. 4 schematically shows a PEM fuel cell and its various components in two-dimensional domain: the anode gas channel, anode gas-diffusion layer, anode catalyst layer, polymer electrolyte membrane, cathode catalyst layer, cathode gas-diffusion layer, and cathode gas channel. Fully humidified fuel and air are fed into the gas channels. Electrochemical reactions are considered to occur only within the active catalyst layers where Pt/C catalysts are intermixed uniformly with recast ionomer. Stoichiometric flow ratio determines the fuel and oxidant flow rates:

$$\varsigma_c = \frac{C_{O2,i} U_{c,i} A_{c,i}}{\frac{I_{cell}}{4F} A_{rx}} \tag{8}$$

$$\varsigma_a = \frac{C_{H2,i} U_{a,i} A_{a,i}}{\frac{I_{cell}}{2F} A_{rx}} \tag{9}$$

Other governing properties describing the mass transfer and electrochemical reactions are taken from

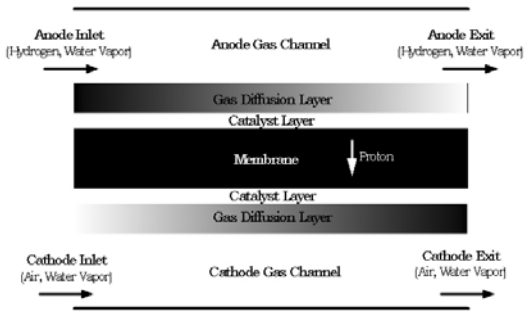

(a) Two-dimensional schematic

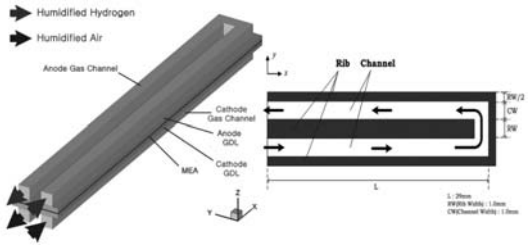

(b) Three-dimensional serpentine geometry

Fig. 4. A computational domain for a fuel cell modeling; (a) two-dimensional schematic, (b) three-dimensional serpentine geometry.

Um et al. [7]

The following assumptions are applied to the present model:

- steady state
- ideal gas mixtures
- incompressible and laminar flow due to small pressure gradients and Reynolds number in the channel flow
- negligible ohmic drop in the electronically conductive solid matrix of porous diffusion and catalyst layers
- constant uniform temperature due to the negligible temperature build-up for a single cell
- water in the vapor phase and/or mist flow modeling
- isotropic and homogeneous electrodes, catalyst layers, and membrane.

2.3 Governing equations

The single-domain approach developed by Um et al.[7] is employed for three-dimensional flow as shown in Fig. 4 and the electrochemical reactions described as source terms in Table 2. Non-linear, partial differential equations representing the conservation of mass, momentum, species, and charge are strongly coupled to account for the transport and elec-

Table 2. Basic operating conditions for the computational study.

Description	Symbol	Value
Cell temperature	T_{cell}	50 °C
Operating cell voltage	V_{cell}	*
Pressure at the gas channel inlet of the anode side	P_a	1.0 atm
Hydrogen mole fraction at the anode gas channel inlet	$C_{a,i}^{H2}$	*
Water vapor mole fraction at the anode gas channel inlet	$C_{a,i}^{W}$	*
Stoichiometry ratio in the anode gas channel	ζ_a	1.5
Stoichiometry ratio in the cathode gas Channel	P_c	1.0 atm
Oxygen mole fraction at the cathode gas channel inlet	$C_{c,i}^{O2}$	*
Nitrogen mole fraction at the cathode gas channel inlet	$C_{c,i}^{N2}$	*
Water vapor mole fraction at the cathode gas channel inlet	$C_{c,i}^{W}$	*
Stoichiometry ratio in the cathode gas channel	ζ_c	3.0

Table 3. Design parameters for the computational study.

Description	Symbol	Value
Cell/electrode length	L	6.1 cm
Gas channel height	CW	0.1 cm
Gas channel width	RW	0.1 cm
Current collector width	*	0.1 cm
Anode catalyst layer thickness	*	0.001 cm
Membrane thickness	Nafion® 112	0.00508 cm
Cathode catalyst layer thickness	*	0.001 cm

trochemical reactions in polymer electrolyte fuel cells.

The governing equations are written in the vector form for the steady-state as [7]

$$\nabla\cdot\left(\rho\vec{u}\right)=0 \tag{10}$$

$$\nabla\cdot\left(\rho\vec{u}\vec{u}\right)=-\nabla P+\nabla\cdot\left(\mu\nabla\vec{u}\right)+S_u \tag{11}$$

$$\nabla\cdot\left(\rho\vec{u}C_k\right)=\nabla\cdot\left(D_k\nabla C_k\right)+S_k \tag{12}$$

$$\nabla\cdot\left(\kappa_e\nabla\Phi_e\right)+S_\Phi=0 \tag{13}$$

where $\vec{u}$, P, C_k, Φ_e, and S represent the intrinsic fluid velocity vector, pressure, molar concentration of chemical species k, the phase potential of the electrolyte membrane, and source terms for the conservation equations, respectively. Basic operating conditions and design parameters for the computational study are listed in Tables II and III. More detailed information on the simulation can be found in the literature [7].

Thermodynamic open circuit potential for the overall fuel cell reaction and the exchange current density for the oxygen reduction reaction are defined [14],

$$V_{oc}=V_{oc}^{ref}+\frac{RT}{2F}\left(\ln P_{\mathrm{H2}}+\frac{1}{2}\ln P_{\mathrm{O2}}\right), \tag{14}$$

where V_{oc}^{ref} represents the sole temperature effect on the open-circuit potential. This can be written,

$$V_{oc}^{ref}=1.2334-0.83\times10^{-3}\left(T-303.15\right) \tag{15}$$

The reference exchange current density at a cell temperature takes the following modified Arrhenius form:

$$aj_{o,c}^{ref}\left(T\right)=aj_{o,c}^{ref}\left(353K\right)\cdot\exp\left[-20000\times\left(\frac{1}{T}-\frac{1}{353.15}\right)\right] \tag{16}$$

The sink/source term describing the water production by the catalytic reaction as well as the electro-osmotic drag from the anode to cathode electrodes can be described as,

$$S_w=\nabla\cdot\left(\frac{n_d}{F}\vec{i}_e\right)\quad\text{for anode} \tag{17}$$

$$S_w=\frac{j_c}{2F}+\nabla\cdot\left(\frac{n_d}{F}\vec{i}_e\right)\quad\text{for cathode} \tag{18}$$

The local current density in the mid-section of the membrane can be calculated as follows:

$$I\left(y,z\right)=-\kappa_e^{eff}\left.\frac{\partial\Phi_e}{\partial x}\right|_{x=M.M.} \tag{19}$$

where the subscript M.M represents the mid-section in the membrane. The average current density is then determined from

$$I_{avg}=\frac{1}{A_{rx}}\int_A I\left(y,z\right)dA_{rx} \tag{20}$$

where A_{rx} is the electrode geometrical area.

Additional modifications are made in order to account for the electrical resistance,

$$\Delta V_{e,R}=I_{avg}\cdot R \tag{21}$$

Where $\Delta V_{e,R}$ and R represent the additional voltage loss by the electrical contact resistance and the electrical resistance obtained from the experiment, respectively.

The corresponding final cell voltage can be computed,

$$V_{cell} = V_{oc} - \Delta V_{ohmic} - \Delta V_{act} - \Delta V_{mass} - \Delta V_{e,R} \quad (22)$$

On the right side of Eq. (22), all other terms are calculated except $\Delta V_{e,R}$ in the computing process.

2.4 Boundary conditions

Eqs. (10)-(13) form a complete stet of governing equations for (m+5) unknowns, where m is the physical dimension of the problem: $\vec{u}$, P, C_{H2}, C_{O2}, C_w, and Φ_e. Due to the single-domain formulation, boundary conditions are required only at the external surfaces of the computational domain. For mass flow, the no-slip and impermeability conditions are applied to all external surfaces except for the inlets and outlets of the anode and gas channels. At the fuel and oxidant inlets, the following conditions are prescribed.

$$\begin{aligned} &u_{a,i} = U_{a,i}, \quad u_{c,i} = U_{c,i} \\ &C_a^{H2} = C_{a,i}^{H2}, \quad C_a^W = C_{a,i}^W \\ &C_c^{O2} = C_{c,i}^{O2}, \quad C_c^W = C_{c,i}^W \end{aligned} \quad (23)$$

where inlet velocities are determined from Eqs. (8) and (9), and the inlet species concentration is calculated by using the ideal gas law under a given operating condition.

2.5 Numerical implementation

For numerical testing, a 180 degree turn single channel is considered. The polymer electrolyte fuel cell model described above is implemented into a commercial computational fluid dynamics (CFD) package, Fluent® by using user-defined functions (UDFs). A series of customized external UDFs are encoded and interlinked to solve the transport and electrochemical reactions in polymer electrolyte fuel cells. Structured, orthogonal meshes are used for all computational meshing. We found that 62x150x30 is sufficient for three-dimensional geometry as shown in Fig. 4. The computation is assumed to be converged when the overall mass balance and species mass balances are met and the relative error between the consecutive iterations is less then 10^{-6}.

3. Results and discussion

Fig. 5 shows the effect of the clamping pressure on the GDL thickness and porosity variations. A sampled 10 BB carbon paper has 420 μm of thickness before compression at its initial state. The carbon paper was compressed to the maximum 50% variation (i.e., ~ 200 μm) of its thickness. As shown in Fig. 5, the compressed thickness of carbon paper used in this study has relatively stiff gradient in the low range of the external clamping pressure (i.e., ~ 5 bar), resulting in the relatively sharp decrease in porosity. In the remaining compression pressure ranges, the porosity of the carbon paper is inversely proportional to the external clamping pressure. Fig. 6 represents the corresponding permeability change under the same condition as shown in Fig. 5. As the applied clamping pressure increases, the permeability shows exponentially decreasing pattern. In Fig. 6, 5 bar of external pressure makes approximately 50% change in gas permeability. When the carbon paper further goes through more than 30 bar of the clamping pressure, the permeability reduces down to 1/10 of the initial value.

Fig. 7 displays the variation of the electronic resistance as a function of the clamping pressure. The

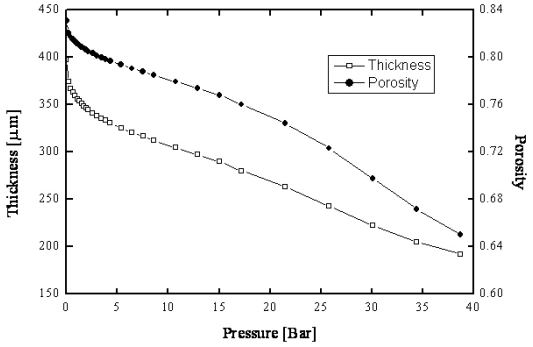

Fig. 5. Effect of the clamping pressure on the variation of the GDL thickness and porosity.

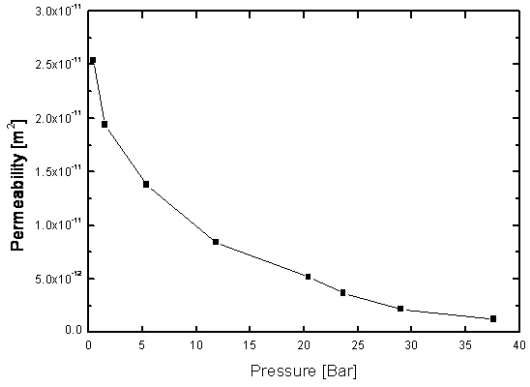

Fig. 6. Effect of the clamping pressure on the variation of the GDL permeability.

electrical resistance is sharply reduced with a slight external clamping pressure from 1800 mΩ·cm^2 at the initial state to 150 mΩ·cm^2 at 2.5 bar, and then shows an asymptotic curve converging on 20 mΩ·cm^2 of the electrical resistance. In general, a fully hydrated Nafion® 112 membrane has an electrical resistance of 70 mΩ·cm^2 in the literature. Therefore, it is evident that the interfacial contact resistance could be a considerable amount of electrical loss of fuel cells, and thus it is necessary to clamp a fuel cell stack closely together, at least more than 10 bar. In addition, it should be noted that for exact understanding of the effect of the clamping pressure on the electrical resistance change, the adoption of electrochemical impedance spectroscopy by fitting to an equivalent circuit should be performed in parallel with this analysis, which is beyond the scope of this macroscopic approach.

A critical factor for optimal fuel cell performance is the permeability which has a strong effect on mass transfer in terms of reactant supply and the water removal to/from the active reaction site. Fig. 8 shows the porosity variation of the sampled carbon paper as a function of carbon paper thickness. In the natural state without external pressure, the carbon paper normally has 80% of porosity. As the clamping pressure increases, the slope of the porosity curve shows an adverse logarithmic pattern, indicating that the carbon paper has a mild deformation in porosity with less thickness change and then severe shrinkage in the pore volume under the high clamping pressure range. It should be also noted that large porosity facilitates the mass diffusion through a porous medium, providing sufficient amounts of reactants to the catalyst layer. The external clamping load to a fuel cell stack results in the deflation of the vacant space of the porous carbon paper.

Fig. 9 shows the performance curves for a single cell experiment with various GDL thicknesses. The ionomer membrane is assumed to be fully saturated with 100% humidified fuel and oxidant feed stream. The measured polarization curves can be taken to reflect the effect of the interfacial electrical resistance and mass transfer since the ionic conductivity has negligible variance under this operating condition. It is shown in Fig. 9 that the fuel cell performance appears worst with 330 μm of the compressed carbon paper thickness. Interestingly, the corresponding polarization curve shows the maximum limiting current density favorable from the mass transfer point of view. For a case of 300 μm compression of GDL, it is shown that the interfacial electrical resistance gets smaller than for the case of 330μm compression and the maximum current density is limited to 1.2 A/cm^2

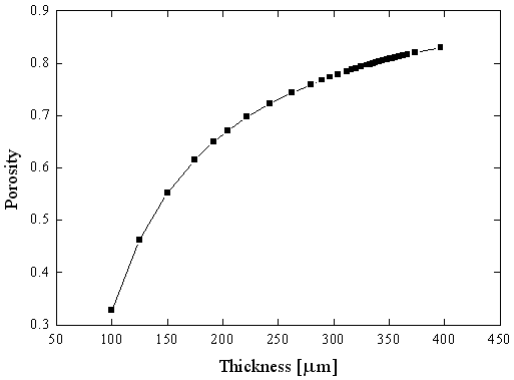

Fig. 8. Effect of the GDL compression on the porosity variation.

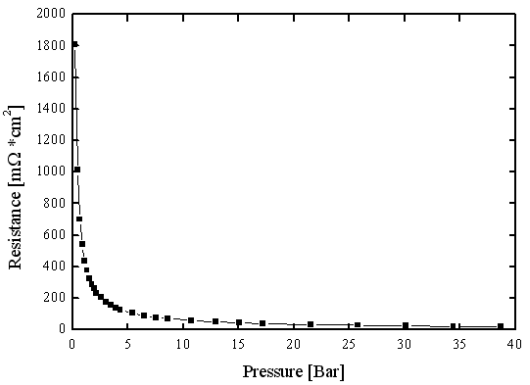

Fig. 7. Effect of the clamping pressure on the variation of the electronic resistance.

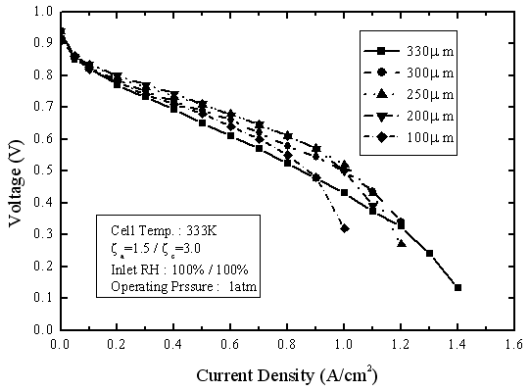

Fig. 9. Performance curves of PEFCs from experiment at various compression levels.

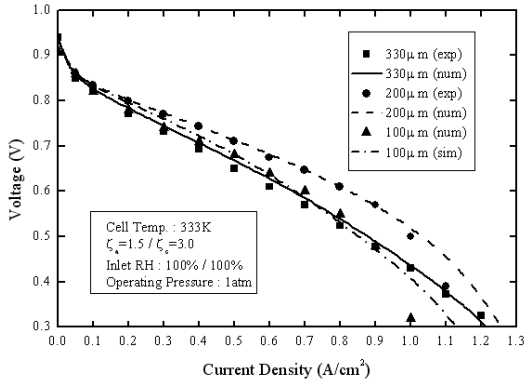

Fig. 10. Comparison of experimental and computational results with the electrical contact resistance considered.

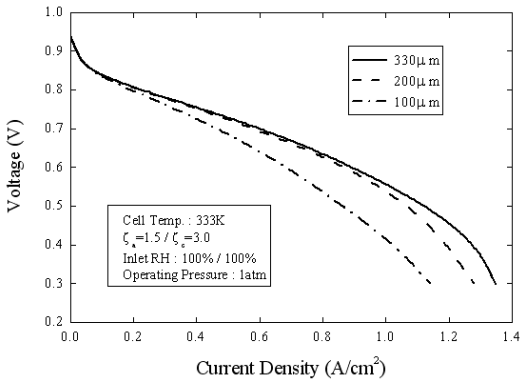

Fig. 11. Computed polarization curves of PEFCs without considering the interfacial contact resistance.

compared to 1.4 A/cm^2 for the 330 μm compression case. Compression between 200 μm and 250 μm shows the highest performance and negligible difference in the performance curve between them. With further compression of 100 μm carbon paper, it seems to be difficult to achieve more than 1.0 A/cm^2 of current density, due mainly to the worst mass transfer limitation. Therefore, it can be concluded that the compression of carbon paper between 200 μm and 250 μm is the favorable clamping thickness of the carbon paper.

The computational polarization curves considering the interfacial contact resistance are compared in Fig. 10 with a series of experimental data under the same operating conditions. The calculated polarization curves show good agreement with the measured experimental data for the polarization curve except in the high current density close to the mass transfer limited region in which the water flooding has a detrimental effect on the fuel cell performance. Fig. 11 shows the calculated polarization curves without considering the electrical contact resistance. For these cases, the fuel cell performance is only affected by the extent of mass transfer from gas channels to active catalyst layers. It is shown in Fig. 11 that the compression effect on the cell polarization is remarkable for a case of 100 μm thickness of carbon paper. More than 200 μm of the compressed carbon paper (i.e., less compression pressure) does not make significant deviation in the predicted cell performances.

4. Conclusions

Experimental and numerical studies were performed to investigate the effect of the clamping pressure on the fuel cell performance. Gas diffusion layers were compressed with various clamping pressures to measure the variation of material properties--porosity, permeability, and electrical conductivity--as a function of the stack clamping pressure or the GDL thickness. The experimental results showed that the porosity of the carbon paper is inversely proportional to the external clamping pressure and more than 50% change in gas permeability appeared with slight external pressure. It was also found that further GDL compression of more than 30 bar in the stack clamping pressure significantly reduces down to 1/10 of permeability from its natural state. The experimental results revealed that the interfacial electrical contact resistance is a considerable electrical loss of fuel cells and the highest fuel cell performance can be obtained with 200-250 μm of the GDL thickness.

Good agreement between the numerical simulation results and experimental measurements was achieved, accounting for the clamping effects on the fuel cell performance. A slight deviation between the experiment and the computed results appeared in the limiting current density regime in which the water flooding should be carefully considered. It could be inferred from this study that less compression (i.e., 300 μm) could possibly promote multi-directional gas diffusion, while inducing worse interfacial electrical resistance. Therefore, it should be noted that the optimal compression level should be determined based on the competing effects among mass transfer and interfacial resistance.

Nomenclature

A_{rx} : Active area, cm^2

$A_{a/c,i}$: Gas channel cross-sectional area, cm^2
C : Molar concentration, mol/cm^3
D : Mass diffusivity of species, cm^2/sec
F : Faraday constant, C/e-mol
I : Current density, A/cm^2
j : Transfer current, A/cm^3
k : Permeability, m^2
L : Gas channel length, cm
M : Molecular weight, g/mol
n_d : Electro-osmotic drag coefficient
P : Pressure, Pa
R : Gas constant, 8.314 J/mol·K
T : Cell temperature, K
$\vec{u}$: Velocity vector, cm/sec

Greek letters

Φ : Phase potential, V
κ : Ionic conductivity, S/m
λ : Water content, mol H_2O/mol SO^{3-}
ζ : Stoichiometric flow ratio, Eq.(1)

Superscripts

eff : Effective value
ref : Reference value
W : Water, H_2O

Subscripts

a : Anode
c : Cathode
e : Electrolyte phase
i : Gas channel in
oc : Open circuit

References

[1] W.-K. Lee, C.-H. Ho, J. W. Van Zee and M. Murthy, The Effects of Compression and Gas Diffusion Layers on the Performance of a PEM Fuel Cell, *J. Power Sources* 84 (1999) 45-51.
[2] M. Mikkola, Experimental Studies on Polymer Electrolyte Membrane Fuel Cell Stacks, M.S.Thesis, Helsinki Univ. of Tech., Finland, (2001).
[3] E. A. Cho, U. S. Jeon, H. Y. Ha, S. A. Hong and I. H. Oh, Characteristics of composite bipolar plates for polymer electrolyte membrane fuel cells, *J. Power Sources* 125 (2004) 178-182.
[4] H. Wang and J. A. Turner, Ferritic stainless steels as bipolar plate material for polymer electrolyte membrane, *J. Power Sources* 128 (2004) 193-200.
[5] S. Um, C. Y. Wang and K. S. Chen, Computational Fluid Dynamics Modeling of Proton Exchange Membrane Fuel Cells, *J. Electrochem. Soc.* 147 (2000) 4485-4493.
[6] V. Gurau, H. Liu and S. Kakac, Two-Dimensional Model for Proton Exchange Membrane Fuel Cells, *AIChE J.* 44 (11) (1998) 2410-2422.
[7] S. Dutta, S. Shimpalee and J. W. Van Zee, Three-Dimensional Numerical Simulation of Straight Channel PEM Fuel Cells, *J. Appl. Echectrochem.* 30 (2000) 135-146.
[8] S. Um, Computational Modeling of Transport Phenomena and Electrochemical Kinetics in Proton Exchange Membrane Fuel Cells, Ph. D. Thesis, The Pennsylvania State University, USA, (2003).
[9] H. Meng and C. Y. Wang, Electron Transport in PEFCs, *J. Electrochem. Soc.* 15 (2004) A358-A367.
[10] T. Berning, D. M. Lu and N. Djilali, Three-Dimensional Computational Analysis of Transport Phenomena in a PEM Fuel Cell, *J. Power Sources* 106 (2002) 284-294.
[11] N. P. Siegel, M. W. Ellis, D. J. Nelson and M. R. von Spakovsky, A Two-Dimensional Computational Model of a PEMFC with Liquid Water Transport, *J. Power Sources* 128 (2) (2004) 173-184.
[12] D. Natarajan and T. Van Nguyen, Three-Dimensional Effects of Liquid Water Flooding in the Cathode of a PEM Fuel Cell, *J. Power Sources* 115 (1) (2003) 66- 80.
[13] U. Pasaogullari and C. Y. Wang, Two-phase Transport and the Role of Micro-Porous Layer in Polymer Electrolyte Fuel Cells, *Electrochimica Acta*, 49 (2004) 4359-4369.
[14] A. Parthasarathy, S. Srinivasan and A. J. Appleby, Pressure dependence of the oxygen reduction reaction at the platinum microelectrode/nafion interface: electrode kinetics and mass transport, *J. Electrochem. Soc.* 139 (1992) 2856-2862.

Appendix A

Consider Darcy's Law,

$$u = -\frac{k}{\mu}\nabla P \tag{A-1}$$

where u represents the radial velocity vector, k the gas permeability, μ the molecular viscosity, and P pressure, respectively.

Considering the radial direction only,

$$\frac{\partial P}{\partial r} = -\frac{k}{\mu} u_r \tag{A-2}$$

The radial velocity vector is given as follows:

$$u_r = \frac{1}{2\pi r h} \cdot \frac{R_u T}{PM} \cdot Q \tag{A-3}$$

where h represents the thickness of the carbon paper, R_u the universal gas constant, T temperature, M molecular weight, and Q the gas flow rate, respectively.

Combining Eqs. (A-2) and (A-3),

$$\frac{\partial P}{\partial r} = -\frac{\mu}{k} \cdot \frac{1}{2\pi r h} \cdot \frac{R_u T}{PM} \cdot Q \tag{A-4}$$

Integrating Eq. (A-4) and arranging,

$$k = \frac{1}{\pi h} \cdot \frac{\mu}{P_1^2 - P_2^2} \cdot \frac{R_u T Q}{M} \ln\left(\frac{r_2}{r_1}\right) \tag{A-5}$$

The gas permeability of a porous media can be determined by using Eq. (A-5) in which P_2 corresponds to the ambient pressure in Fig. A-1. The porosity of a porous medium can be derived by using Eq. (A-5) and the Carman-Kozeny relation [21]:

$$k = \frac{\varepsilon^3 d_g^2}{180(1-\varepsilon)^2} \tag{A-6}$$

where ε is the porosity of the porous medium and d_g is the average diameter of the theoretical granules the medium(~20 μm), respectively. The fabrication method of granules can be found in the literature[22]. Strictly, this equation can be used for small porosity medium where the pores have little interaction with one another. In contrast, GDL in PEFCs have high pore spaces more than 60%, and Eq. (A-6) has a limited applicable range in predicting the correct behavior of permeability in fibrous media. Nonetheless, it can be widely used for small changes in porosity.

Porosity, which represents as the volume fraction of the pore spaces to the total volume of the porous medium as a function of permeability by the Carman-Kozeny relation in Eq. (A-6), is closely related to mass transfer by way of the mass diffusivity,

$$D_k^{eff} = \varepsilon^{1.5} \cdot D_k \tag{A-7}$$

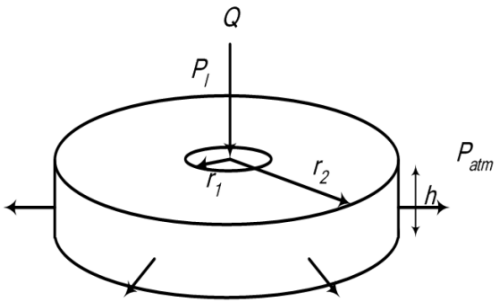

Fig. A-1. A conceptual diagram illustrating permeability measurement.